Spike-Dependent Opsonization Indicates Both Dose-Dependent Inhibition of Phagocytosis and That Non-Neutralizing Antibodies Can Confer Protection to SARS-CoV-2

Wael Bahnan, Sebastian Wrighton, Martin Sundwall, Anna Bläckberg, Olivia Larsson, Urban Höglund, Hamed Khakzad, Magdalena Godzwon, Maria Walle, Elisabeth Elder, et al.

▶ **To cite this version:**

Wael Bahnan, Sebastian Wrighton, Martin Sundwall, Anna Bläckberg, Olivia Larsson, et al.. Spike-Dependent Opsonization Indicates Both Dose-Dependent Inhibition of Phagocytosis and That Non-Neutralizing Antibodies Can Confer Protection to SARS-CoV-2. Frontiers in Immunology, 2022, 12, 10.3389/fimmu.2021.808932 . hal-04430479

HAL Id: hal-04430479
https://hal.science/hal-04430479v1

Submitted on 31 Jan 2024

HAL is a multi-disciplinary open access archive for the deposit and dissemination of scientific research documents, whether they are published or not. The documents may come from teaching and research institutions in France or abroad, or from public or private research centers.

L'archive ouverte pluridisciplinaire **HAL**, est destinée au dépôt et à la diffusion de documents scientifiques de niveau recherche, publiés ou non, émanant des établissements d'enseignement et de recherche français ou étrangers, des laboratoires publics ou privés.

frontiers in Immunology

ORIGINAL RESEARCH
published: 14 January 2022
doi: 10.3389/fimmu.2021.808932

Spike-Dependent Opsonization Indicates Both Dose-Dependent Inhibition of Phagocytosis and That Non-Neutralizing Antibodies Can Confer Protection to SARS-CoV-2

Wael Bahnan[1], Sebastian Wrighton[1], Martin Sundwall[1], Anna Bläckberg[1,2], Olivia Larsson[3], Urban Höglund[3], Hamed Khakzad[4,5], Magdalena Godzwon[6], Maria Walle[6], Elisabeth Elder[7], Anna Söderlund Strand[8], Lotta Happonen[1], Oscar André[1], Johannes Kumra Ahnlide[1], Thomas Hellmark[9], Vidar Wendel-Hansen[10], Robert PA. Wallin[11], Johan Malmstöm[1], Lars Malmström[1,12], Mats Ohlin[6,13], Magnus Rasmussen[1,2] and Pontus Nordenfelt[1]**

[1] Department of Clinical Sciences Lund, Infection Medicine, Faculty of Medicine, Lund University, Lund, Sweden, [2] Infectious Disease Clinic, Skåne University Hospital, Lund, Sweden, [3] Adlego Biomedical AB, Uppsala, Sweden, [4] Equipe Signalisation Calcique et Infections Microbiennes, Ecole Normale Supérieure Paris-Saclay, Gif-sur-Yvette, France, [5] Institut National de la Santé et de la Recherche Médicale (INSERM) U1282, Gif-sur-Yvette, France, [6] Department of Immunotechnology, Lund University, Lund, Sweden, [7] Public Health Agency of Sweden, Solna, Sweden, [8] Department of Laboratory Medicine, Clinical Microbiology, Skane University Hospital Lund, Lund University, Lund, Sweden, [9] Department of Clinical Sciences Lund, Nephrology, Skane University Hospital Lund, Lund University, Lund, Sweden, [10] Tanea Medical Ab, Uppsala, Sweden, [11] SciEd Solutions, Stockholm, Sweden, [12] Institute for Computational Science, Zurich, Switzerland, [13] SciLifeLab Drug Discovery and Development, Lund University, Lund, Sweden

Spike-specific antibodies are central to effective COVID19 immunity. Research efforts have focused on antibodies that neutralize the ACE2-Spike interaction but not on non-neutralizing antibodies. Antibody-dependent phagocytosis is an immune mechanism enhanced by opsonization, where typically, more bound antibodies trigger a stronger phagocyte response. Here, we show that Spike-specific antibodies, dependent on concentration, can either enhance or reduce Spike-bead phagocytosis by monocytes independently of the antibody neutralization potential. Surprisingly, we find that both convalescent patient plasma and patient-derived monoclonal antibodies lead to maximum opsonization already at low levels of bound antibodies and is reduced as antibody binding to Spike protein increases. Moreover, we show that this Spike-dependent modulation of opsonization correlate with the outcome in an experimental SARS-CoV-2 infection model. These results suggest that the levels of anti-Spike antibodies could influence monocyte-mediated immune functions and propose that non-neutralizing antibodies could confer protection to SARS-CoV-2 infection by mediating phagocytosis.

Keywords: antibodies, SARS – CoV – 2, antibody function, antibody binding, spike (S) protein, phagocytosis, *in vivo* model

OPEN ACCESS

Edited by:
Penghua Wang, University of Connecticut Health Center, United States

Reviewed by:
Zhanbo Zhu, Heilongjiang Bayi Agricultural University, China
Jianfeng Dai, Soochow University, China

****Correspondence:***
Pontus Nordenfelt
pontus.nordenfelt@med.lu.se
Wael Bahnan
wael.bahnan@med.lu.se

Specialty section:
This article was submitted to Viral Immunology, a section of the journal Frontiers in Immunology

Received: *04 November 2021*
Accepted: *21 December 2021*
Published: *14 January 2022*

Citation:
Bahnan W, Wrighton S, Sundwall M, Bläckberg A, Larsson O, Höglund U, Khakzad H, Godzwon M, Walle M, Elder E, Strand AS, Happonen L, André O, Ahnlide JK, Hellmark T, Wendel-Hansen V, Wallin RPA, Malmstöm J, Malmström L, Ohlin M, Rasmussen M and Nordenfelt P (2022) Spike-Dependent Opsonization Indicates Both Dose-Dependent Inhibition of Phagocytosis and That Non-Neutralizing Antibodies Can Confer Protection to SARS-CoV-2. Front. Immunol. 12:808932. doi: 10.3389/fimmu.2021.808932

INTRODUCTION

COVID19, caused by the SARS-CoV-2 virus, has since the end of 2019 resulted in millions of deaths and serious societal health effects. Treatment of patients with convalescent plasma or monoclonal antibodies was attempted early on during the pandemic, inspired by previous partial successes with Respiratory Syncytial Virus (1) and Ebola (2). Two monoclonal antibody cocktails targeting the SARS-CoV-2 Spike protein (casirivimab and imdevimab) (3) and (bamlanivimab and etesevimab) (4, 5) were given emergency use authorization by the FDA after positive phase III clinical trial data. Trials showed that antibody cocktails reduced symptoms, hospitalization, and mortality associated with COVID19 for early-stage infections. However, studies regarding their use for treating severe COVID19 showed no clinical benefit (6).

The therapeutic antibodies described previously neutralize the interaction between the Spike protein and the ACE2 receptor, thereby hindering viral entry into host cells. Considerable efforts have been made to generate neutralizing anti-Spike antibodies (7–10). Neutralizing antibodies, however, constitute only a fraction of the antibody repertoire generated by B cells against the Spike protein during COVID19 infection (11). The opsonic capability has not been a focal point in the characterization of neutralizing antibodies. Non-neutralizing antibodies, comprising the majority of the humoral immune response to a pathogen, have other immunological functions such as complement-dependent immune activation and viral phagocytosis [reviewed by Forthal (12)]. Phagocytosis plays a substantial role in the anti-viral immune response (13). Through virion or cellular phagocytosis, phagocytic cells help reduce the viral load by eliminating infection sources. In this context, we were interested in whether or not Spike antibodies might mediate phagocytosis as has been previously seen with influenza (13–15).

However, in other viral infections (such as Dengue, SARS-CoV-2, Respiratory Syncytial Virus, and others), insufficient levels of neutralizing antibodies allow non-neutralizing antibodies to mediate the entry of virions into host immune cells (16). This infection of immune cells *via* FcγR leads to Antibody-Dependent-Enhancement (ADE), exacerbating the infection and worsening patient outcomes (17). So far, studies on COVID19 vaccines and monoclonal antibodies utilized in COVID19 therapy have seen no evidence of ADE (16–21). This clinical absence of ADE remains true even when some studies report that patient sera with high titers of neutralizing antibodies could induce Spike-bead phagocytosis or FcγR-activation (ADCP) (22–24).

Our work shows evidence that convalescent patient plasma and monoclonal anti-Spike antibodies induce phagocytosis but with diminishing returns when the antibody concentrations become high. We also demonstrate that the activation and inhibition of phagocytosis are independent of neutralization potential. Finally, we present data from an experimental animal infection model showing that non-neutralizing antibodies can protect animals from SARS-CoV-2 infection. The results in this study shed light on the importance of non-neutralizing antibodies in mediating phagocytosis and how their presence translates into protection after experimental infection.

RESULTS

Convalescent Patient Plasma Reduces Spike-Monocyte Interaction

Blood plasma was obtained from 20 COVID19 convalescent patients (**Supplementary Table 1**). We used biotinylated Spike protein conjugated to streptavidin fluorescent microspheres (1 μm beads) as a model for Spike-monocyte interactions. The beads were used as bait for THP-1 monocytes. To opsonize the beads, we incubated them with the patient plasma at different dilution levels. We chose the 0.01-1% concentrations to mimic IgG levels in the mucosal niche or tissues, which would be the first place of encounter with the SARS-CoV-2 virus. The highest level of association between plasma-opsonized Spike-beads and cells was at the intermediate plasma dilution (0.1%), while the higher and lower concentrations of plasma (1 and 0.01%, respectively) showed reduced association (**Figure 1A**). In fact, the only consistent effect we saw across our patient plasma samples was a reduction in Spike-particle association with THP-1 cells at the highest plasma concentration. This phenomenon was seen in 18 out of 20 patient samples. Two patient samples (patients 8 and 18) showed no or low opsonic ability. The reduction in Spike-THP-1 cell association under high plasma concentrations was independent of patient sex, age, or disease severity (**Supplementary Table 1**).

As our results were unexpected, we checked whether the reduction in particle-to-cell association seen at higher plasma concentrations (1%) was due to a loss of Spike or antibody binding. For that purpose, we methanol-fixed the phagocytosis samples (cells and beads) from the experiment shown previously (**Figure 1A**). The samples were then stained with a fluorescently conjugated (FITC) secondary antibody (Fab anti-human Fab), which would react with the plasma anti-Spike antibodies which had bound to Spike on the beads. Unsurprisingly, increased plasma concentrations led to increased binding of Spike-specific antibodies to the Spike-beads (**Figure 1B**). In contrast, patients 8 and 18 showed no or very low binding of antibodies to Spike-beads, correlating with overall reduced opsonization (**Figure 1A**). Our results show that when assayed at higher concentrations, patient plasma is not permissive to THP-1 cell-Spike interactions, despite having antibodies that readily bind Spike protein.

Generation of Spike-Reactive Human Monoclonal Antibodies

Considering our previous data showing that high concentrations of COVID19 convalescent plasma reduced Spike-THP-1 cell interactions compared to low concentrations, we decided to identify the role monoclonal antibodies play in Spike-THP-1 cell interactions. We isolated Spike-reactive B cells from convalescent COVID19 patients and performed single-cell

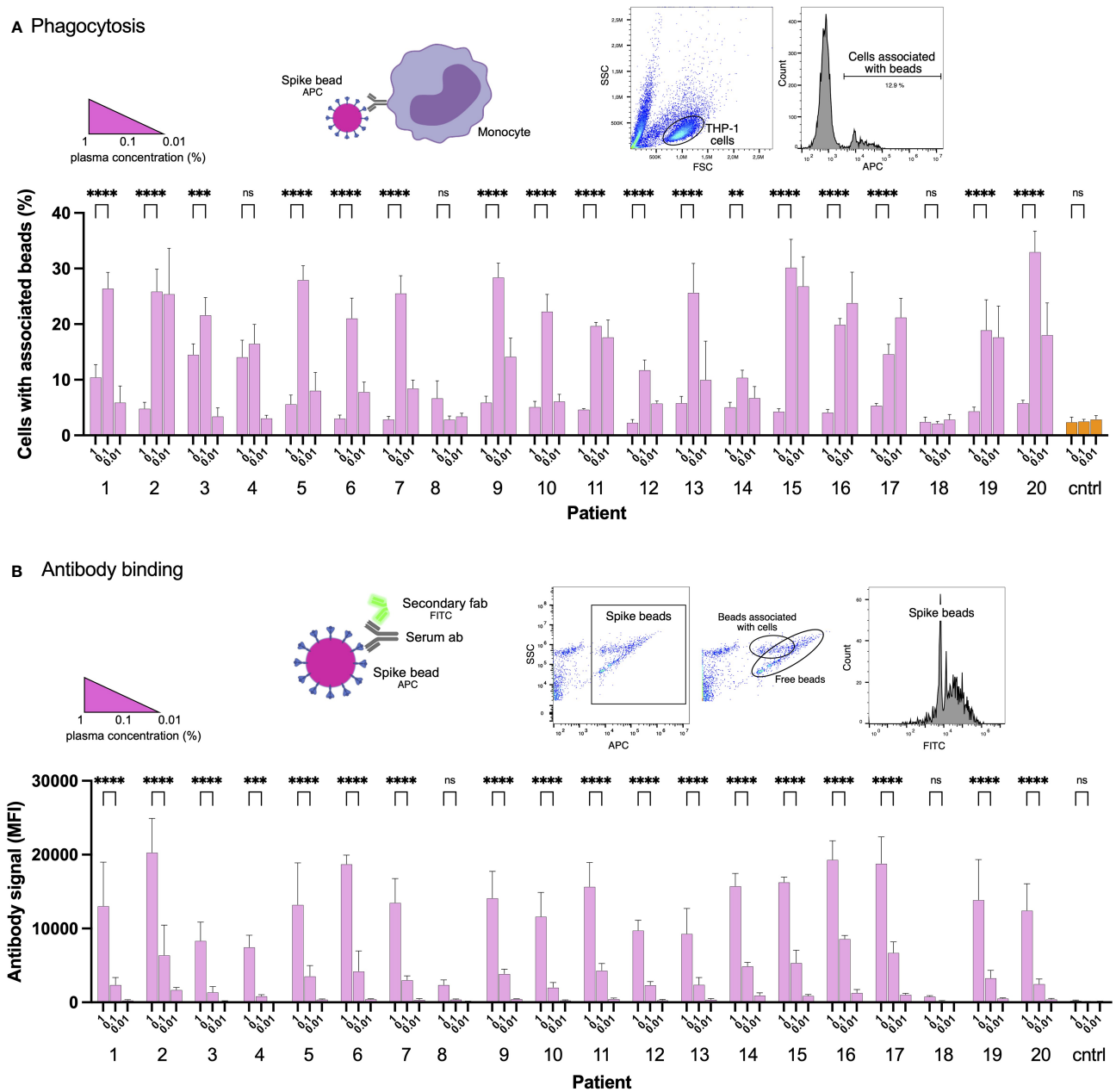

FIGURE 1 | Convalescent patient plasma reduces Spike-monocyte interaction. **(A)** Biotinylated Spike protein was conjugated to fluorescent (APC) streptavidin microspheres and was opsonized with three convalescent patient plasma concentrations (1%, 0.1%, and 0.01%). The beads were then mixed with THP-1 cells at a ratio of 2:1, and the association was measured using flow cytometry. Cells that had signal in the APC channel were considered positive. The gating strategy is shown in the top right. **(B)** The same samples of THP-1 cells and beads from **(A)** were fixed with methanol and stained with a fluorescent (FITC) Fab anti-human Fab secondary antibody. The samples were analyzed for human antibody (opsonin) binding to the Spike-beads using flow cytometry. The gating strategy is shown in the top right. The data presented are from three independent experiments. Error bars represent the SD. Statistical significance was assessed using two-way ANOVA with Dunnett's multiple comparison correction. ** denotes for $p \leq 0.01$, *** for $p \leq 0.001$ and **** for $p \leq 0.0001$. ns, not significant. Created with BioRender.com.

sequencing (**Figure 2A**). We chose 96 antibodies for production that were equidistantly spaced on the genetic clustering tree (**Supplementary Figure 1A**). The antibodies were expressed in HEK293 cells. ELISA-based screening of the antibody-containing supernatants allowed us to identify ten Spike-reactive antibodies (**Figure 2B**, **Supplementary Figures 1B, C**), which belonged to different IgG germlines (**Supplementary Figure 1D**). The Spike-reactive antibodies were then assayed for reactivity against Spike-beads using flow cytometry, where we observed that nine antibodies were reactive to the Spike-beads (**Figure 2C**). Ab11, 57, 59, 66, 77, 81, 94, and 95 showed clear reactivity (>40% positive beads) when assayed with Spike-beads

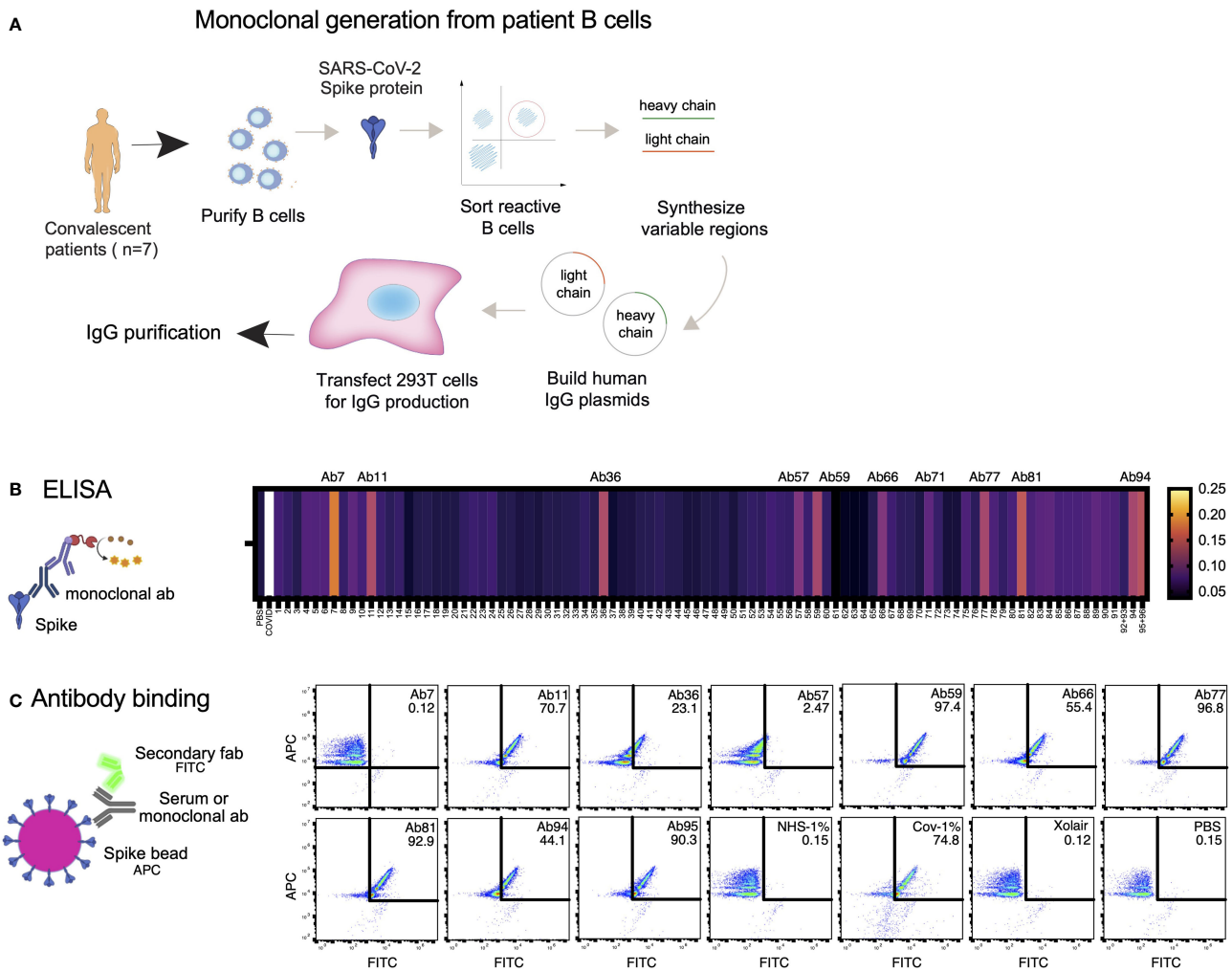

FIGURE 2 | Generation of Spike-reactive human monoclonal antibodies. **(A)** Human monoclonal antibodies were generated from convalescent donor B cells through single-cell sequencing technology. 96 antibodies derived from Spike-reactive human B cells were produced in HEK293F cells. **(B)** Cell culture supernatants containing the antibodies were assayed by ELISA for reactivity against immobilized Spike protein. Serum from a COVID19 patient was used as a positive control (external patient, not from the 20-patient cohort used in **Figure 1**). The data represent three replicate ELISAs where reproducibly reactive antibodies are indicated with their names above the heatmap. **(C)** Antibodies which were Spike-reactive in **(B)** were assayed for reactivity to Spike immobilized on beads. Fluorescent (APC) Streptavidin beads coated with biotinylated Spike protein were incubated with HEK293F-produced antibodies at a concentration of 1 μg/ml. The beads were then stained with a fluorescent (FITC) secondary anti-Fab antibody. The beads were analyzed by flow cytometry. Antibodies that shifted the beads into the FITC-positive gate were deemed reactive. Created with BioRender.com.

at a concentration of 1 μg/ml. Ab59 demonstrated strongest binding, as could be seen through the relative increase in bead staining. Xolair (used at 10 μg/ml) and normal (pre-COVID19) plasma served as negative controls, whereas COVID19 plasma from a convalescent patient was our positive control.

Epitope Mapping and Structural Mass Spectrometry Identify Antibody Binding Sites

To identify antibody binding sites, we first used ELISA to study Spike domain interactions with RBD, RBD with L452R and T478K mutations (delta), and NTD from Spike (**Figure 3A**). We could detect binding to seven antibodies, with high integrated signal (0.2-30 nM titration curves) for Ab59, Ab66, Ab81, and Ab94. Ab66 showed stronger interaction with delta RBD, and Ab 81 showed a lower signal. Ab94 only bound the NTD of Spike. We also performed relative antibody epitope mapping using the single-chain antibody fragments (scFv) isolated from an extensive combinatorial library. scFv mapping revealed that the Ab59 epitope overlaps with those of two scFv (A03_D02 and E01_C09, **Figure 3B**) that interfere in the binding of Spike to ACE2.

Next, we used TX-MS (25) to determine the binding interface between the SARS-CoV-2 specific antibodies and the RBD domain of the Spike protein. In short, we cross-linked the ten antibodies separately to the RBD domain, followed by mass

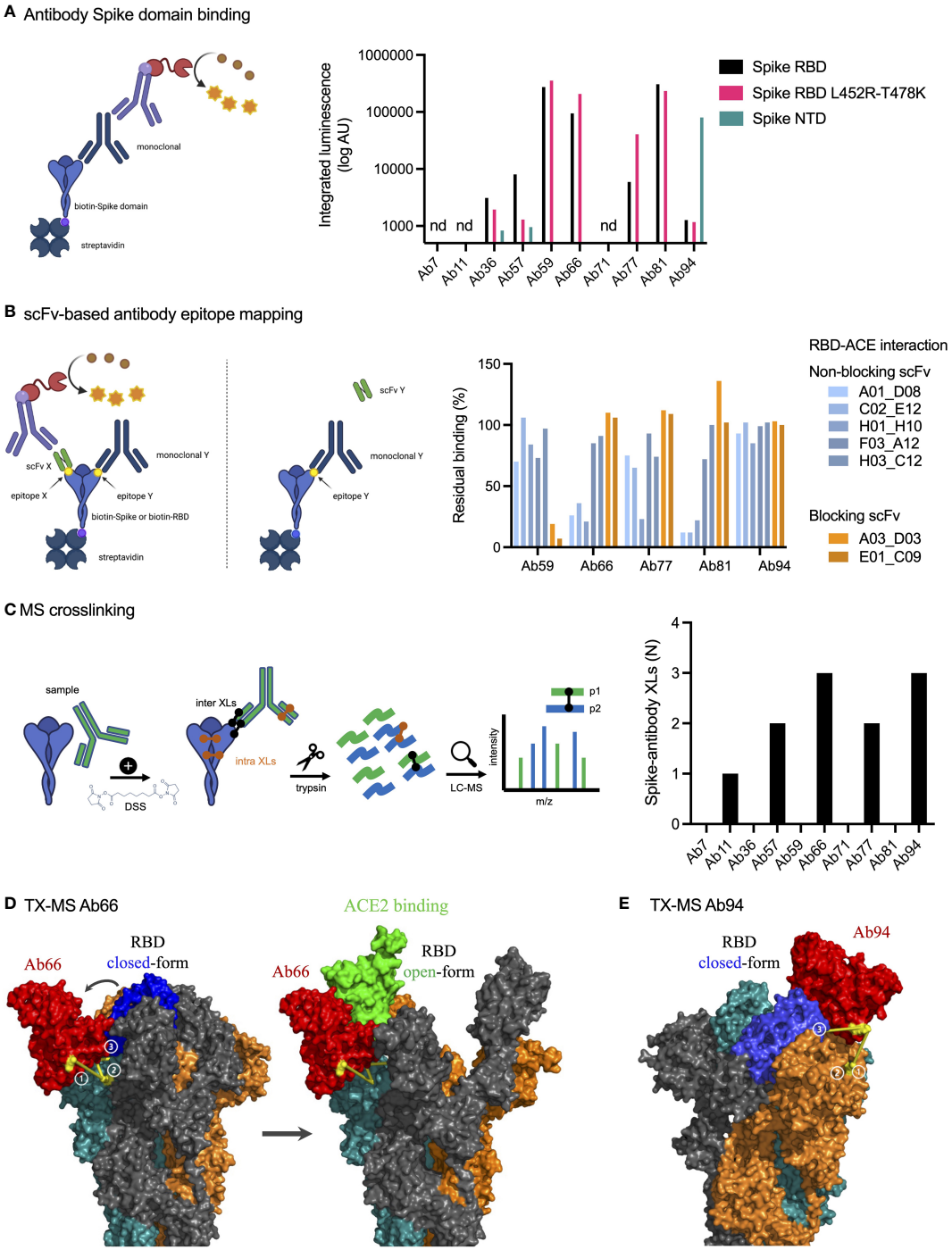

FIGURE 3 | Epitope mapping and structural mass spectrometry identify antibody binding sites. **(A)** Antibody binding to Spike domains was analyzed using ELISA as shown with HRP signal as readout. Antibodies were titrated at 0.2-30 nM, and the integrated signal was calculated. The relative binding to each Spike domain is shown. nd, not determined. **(B)** Epitope mapping was performed using scFvs targeting RBD epitopes as shown. Antibody blocking of scFv binding was measured using anti-FLAG HRP signal. Representative of two independent experiments. **(C)** Spike protein was mixed with anti-spike antibodies and the complex was cross-linked with DSS, allowing for inter and intra cross-links. After trypsinization, mass spectrometric analysis was performed. The table to the right displays the number of inter-protein cross-links detected between Spike and its corresponding antibody. **(D, E)** The binding sites for Ab66 and Ab94 were determined by TX-MS using the cross-links from c, and the data was modelled using Rosetta. Models for Ab66 **(D)** binding the Spike protein in both its open and closed conformations as well Ab94 **(E)** are shown. The cross links between Spike and antibodies are shown in yellow. Created with BioRender.com.

spectrometry analysis and structural modeling (26). This resulted in the identification of 11 confident inter-protein XLs between the RBD domain and five of the antibodies (Ab11, Ab57, Ab66, Ab77, and Ab94) in addition to 30 intra RBD XLs (**Figure 3C**, **Supplementary Figure 2**). The results show that the five antibodies can bind to the Spike protein, but they do not appear to compete with the binding site of human ACE2 directly. The interaction between Ab66 and Spike protein show binding to the open-state but not the closed-state (**Figure 3D**). Further, the structural model indicates no competition between Ab66 and human ACE2, which is in accordance with previously published work, as only the open-state is responsible for binding human ACE2 (27). In contrast, Ab94 appears to preferably bind the closed state (**Figure 3E**). The top and frontal views (with a 180°C rotation) shows the interaction cross-linked sites (**Supplementary Figure 3**). It is important to note that Ab94, after repeated modelling efforts seems to only bind to the closed conformation of Spike. The binding however, does not seem to lock the Spike protein into a closed conformation. Consistent with our other data, even though Ab94 might be able to bind to the RBD, it is non-neutralizing. The combined data from our epitope analysis approaches indicate that Ab11, 57, 59, 66, 77, 81 bind Spike RBD, that Ab94 could interact with both RBD and NTD, and that Ab59 could be a neutralizing antibody, whereas the others are likely non-neutralizing.

Neutralization Assays Identify One Monoclonal Which Blocks the ACE2-Spike Protein Interaction

Typically, the most important biological function attributed to antibodies in the context of a viral infection is neutralization. We assayed our Spike-reactive antibodies for Spike-neutralization using three different approaches: Spike RBD-ACE2 protein binding (**Figure 4A**), Spike particle-ACE2 cell interaction (**Figure 4B**), and SARS-CoV-2 pseudovirus infection neutralization (**Figure 4C**). The SPR-based Spike RBD-ACE2 binding data showed that Ab36 and Ab94 did not appear to interfere with RBD-ACE2 binding and that Ab57 reduced binding slightly. Ab59 completely blocked RBD-ACE binding, whereas Ab66, Ab77, and Ab81 seemed to bind well without interfering with the interaction. Next, we utilized ACE2-expressing HEK293 cells as a surrogate for lung epithelial cells. We measured the ability of Spike-beads to bind HEK293-ACE2+ cells after being opsonized with antibody supernatants. We assayed all 96 of our antibody-containing supernatants for Spike-particle neutralization. Only Ab59 showed a robust and reproducible reduction in Spike-particle binding to HEK293-$ACE2^+$ cells compared to COVID19 patient plasma (**Figure 4B**). As expected, pre-COVID19 plasma showed no inhibition of Spike-ACE2 interactions. Representative images of our experiments which were used for analysis, are shown in **Supplementary Figure 4**. We utilized a pseudovirus binding assay to verify the ability of our antibodies to neutralize SARS-CoV-2. Consistent with our previous experiments with RBD and Spike-beads (**Figures 4A, B**), we saw that Ab59 was the best (EC_{50}: 19 ng/ml) among our antibodies in neutralizing SARS-CoV-2 pseudovirus infection (**Figure 4C**). Taken together, our results indicate that of our 96 antibodies, only Ab59 is a potent neutralizer of the Spike-ACE2 interaction.

High Levels of Human Monoclonal Antibodies Reduce Spike-Monocyte Interaction

Antibodies are the primary mediators of FcγR-dependent cellular interactions. Given our previous data that high concentrations of convalescent patient plasma can reduce Spike-bead association with THP-1 monocytes (**Figure 1**), we tested whether this reduction was antibody-driven. We chose antibody concentrations that were in a similar range (100 - 0.01 μg/ml) than what is expected at the plasma concentrations used (1% - 0.1%) (**Figure 1**) and included a higher plasma concentration for comparison (10%). Interestingly, as with patient blood plasma, serially diluted Spike-specific monoclonal antibodies showed the same inhibition trend of bead-to-cell association at the higher concentrations (**Figure 5A**). This association was confirmed to reflect the internalization of particles (i.e., phagocytosis) by using a pH-dependent fluorescent dye (**Supplementary Figure 5**). Also, as with plasma, this inhibition was correlated with increased antibody binding to Spike (**Figure 5B**). It is important to note here that among the antibodies, Ab94 seemed to have almost half the binding efficiency of Ab59, an attribute that will be central for other experiments. The neutralizing antibody, Ab59, showed the same trend as the other non-neutralizing antibodies. We have thus identified that Spike-specific monoclonal antibodies isolated from COVID19 patients modulate the Spike-THP-1 cell interactions in a dose-dependent manner. This phenomenon is independent of the Spike-ACE2 neutralization capability of the monoclonal antibodies.

Non-Neutralizing Antibodies Can Protect Against SARS-CoV-2 Infection

We have shown that among our antibodies, Ab59 is neutralizing while the other monoclonals are not. We have also demonstrated that our Spike-bead reactive antibodies are efficient at mediating Spike-mediated phagocytosis but reach a threshold after which there is a reduction in interaction efficacy. To test the antibodies' function in a physiologically relevant context, we assessed different doses of neutralizing and non-neutralizing antibodies in an experimental animal infection model (**Figure 6A**). We infected humanized ACE2 mice intranasally with 10^5 PFU (SARS-CoV-2; Wuhan strain from Swedish isolate). As a treatment model, we administered our monoclonal antibodies intraperitoneally a day after infection. Based on previous experience, we used the pseudovirus neutralization data (**Figure 4C**) to calculate a protective dose in a prophylactic model (100 μg for Ab59). To test the effects of high dose administration, Ab59 was given at five times the calculated protective dose. For Ab94, we chose the same dose that would be considered protective for Ab59 (100 μg), as well as a higher dose (250 μg), which would be equivalent to the protective Ab59 dose based on the lower affinity of Ab94 (~2.5 times lower, **Figures 2C** and **5B**). Interestingly, the best-protected animal

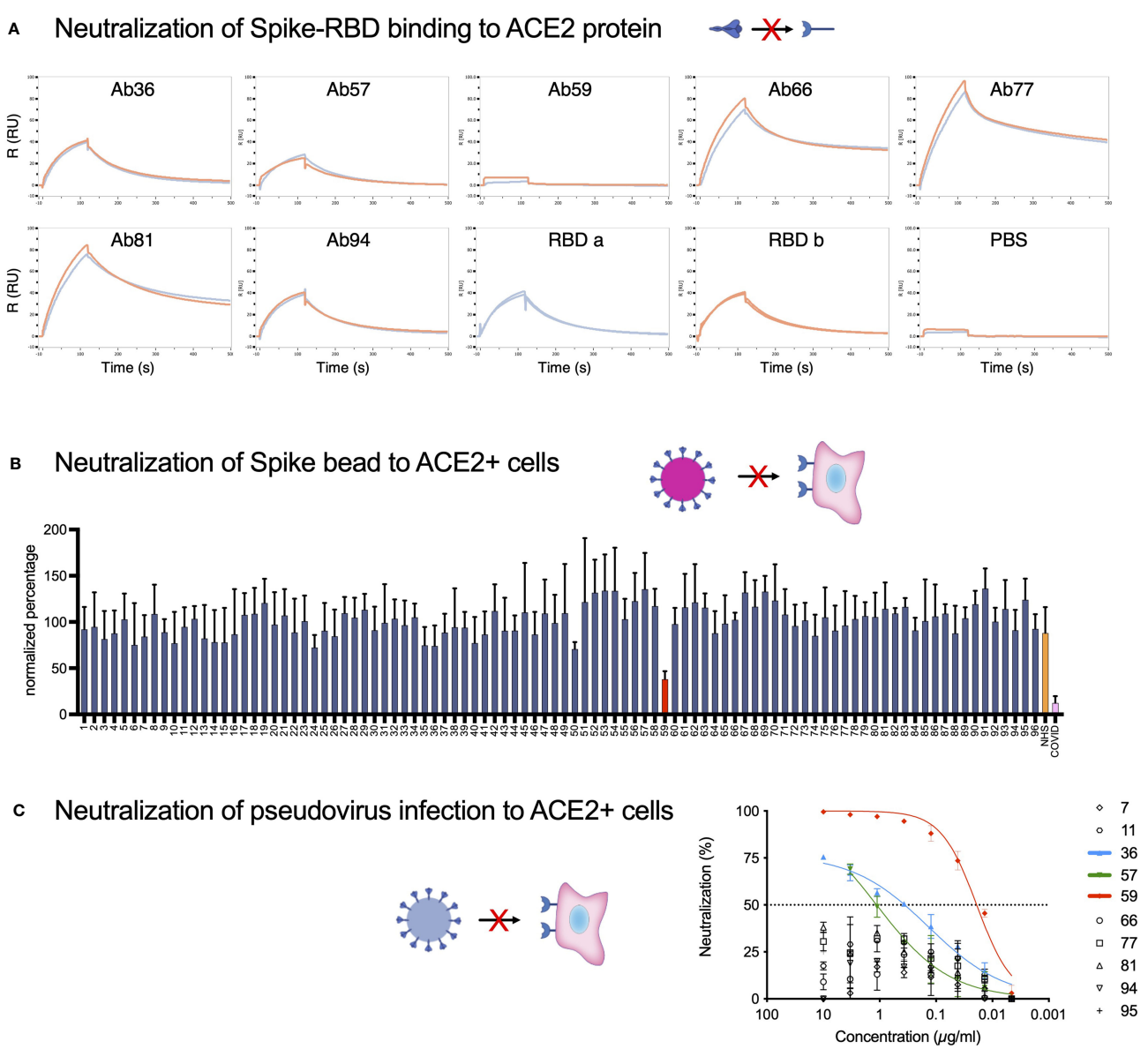

FIGURE 4 | Neutralization assays identify one monoclonal as blocking the ACE2-Spike protein interaction. **(A)** SPR analysis of the binding of monoclonal antibodies to the RBD domain of the Spike protein. PBS served as a negative control, and the intact RBD was our positive control for ACE2 binding. **(B)** The 96 antibodies which we produced were assayed for neutralization potential in a Spike-bead-based neutralization assay. Spike-beads [such as the ones used in **(B)**] were opsonized with the antibodies in 96 well plates. The beads were then centrifuged, reconstituted in fresh media, and added to HEK293-ACE2 cells at a ratio of 20 beads per cell and imaged with automated microscopy. The data is from 4 pooled experiments and is presented as bead association normalized percentage. Error bars indicate the SEM for the replicate experiments. **(C)** The 10 Spike-ELISA reactive antibodies were assayed for pseudovirus neutralization. A firefly luciferase encoding pseudotype lentivirus was used to infect HEK239-ACE2 cells. Antibody serial dilutions were used to block the viral entry into the HEK293-ACE2 cells. Nonlinear regression lines were fitted for the three antibodies that showed a higher than 50% reduction of infectivity. Those antibodies were highlighted in green (Ab57), blue (Ab36), and red (Ab59). Created with BioRender.com.

group (lower weight loss) was the one where the animals were treated with the equivalent to a protective dose of our non-neutralizing yet opsonic Ab94 (**Figure 6B**). Unexpectedly, the animals treated with a low dose of Ab59 fared better than the ones with the high dose, which had the worst outcome (more pronounced weight loss) among the treated groups. The low dose of Ab94 offered negligible improvement compared to untreated animals (**Figure 6B**). The bronchoalveolar lavage (BAL) fluids from the infected mice were harvested and the viral load in the samples were assessed. The cycle threshold (Ct) values in the BAL fluids reflected what the weight loss data showed. The animals which were untreated, or treated with the excessive dose of Ab59 (500 μg) as well as the uncorrected dose for Ab94 (100 μg) faired the worst. Those animals

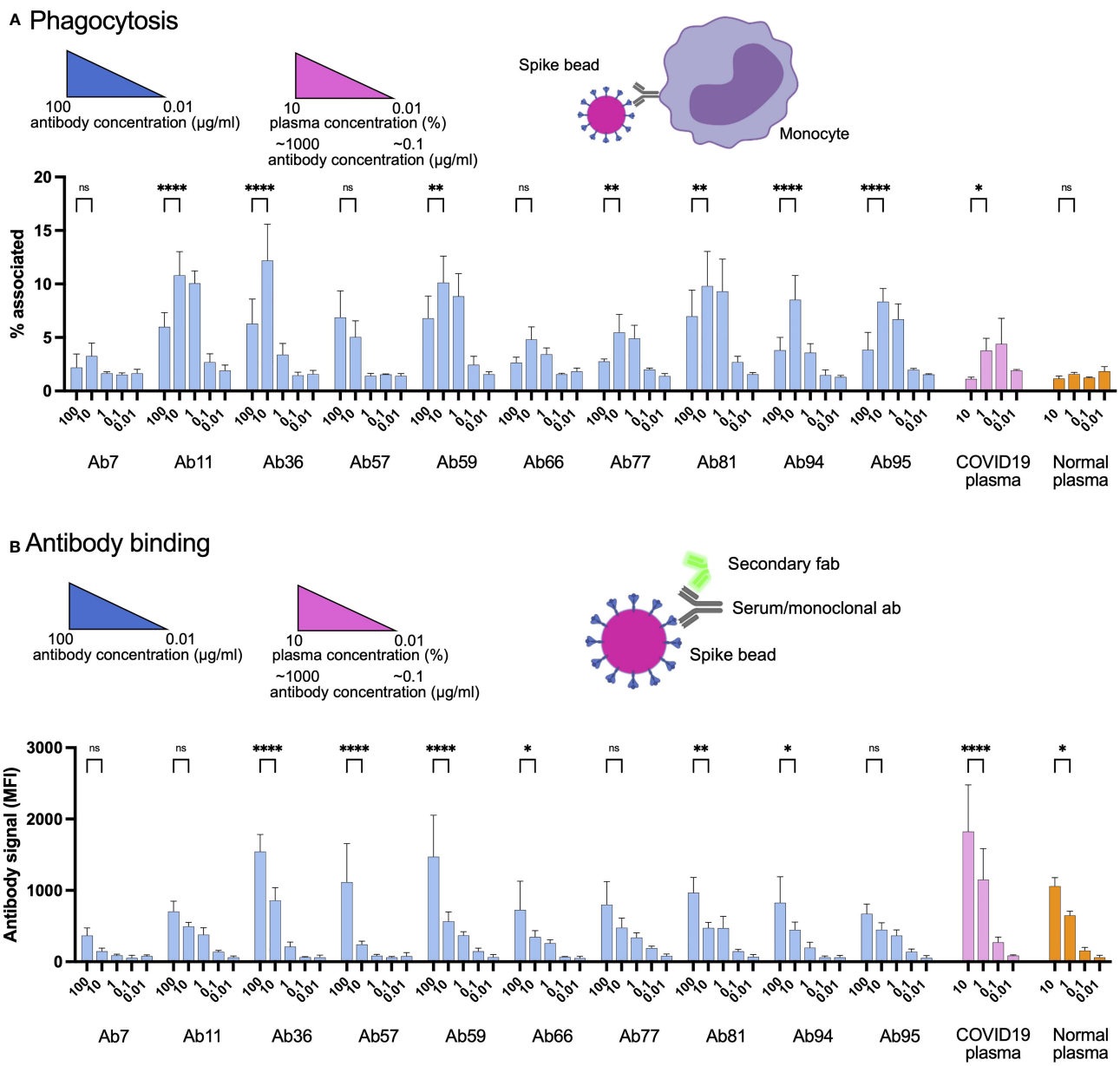

FIGURE 5 | High levels of human monoclonal antibodies reduce Spike-monocyte interaction. **(A)** Spike-reactive monoclonal antibodies at concentrations of 100, 10, 1, 0.1, and 0.01 μg/ml were used to opsonize Spike-beads. Plasma was used at serial dilutions of 10%. The beads were then incubated with THP-1 cells at a ratio of 2 beads/cell. The cells were then analyzed by flow cytometry for association with the fluorescent Spike-beads. The data show the % of bead-associated cells and is pooled from three independent experiments. Error bars represent the SD. **(B)** The cells used in **(A)** were fixed with methanol and restained with a fluorescent (FITC) Fab anti-human secondary antibody. The samples were assessed for human antibody (opsonin) binding to the Spike-beads using flow cytometry. The data are from three independent experiments. Error bars represent the SD. * denotes $p \leq 0.05$, ** for $p \leq 0.01$, and **** for $p \leq 0.0001$. ns, not significant. Created with BioRender.com.

showed the lowest Ct values for SARS-CoV-2 in the BAL fluids, corresponding to the highest titers (**Figure 6C**). Contrastingly, the animals treated with the appropriate doses of Ab94 or Ab59 faired better and showed higher Ct values, corresponding to lower viral loads. The animal data indicate that too high doses of neutralizing antibodies are not beneficial in a treatment model and that non-neutralizing antibodies can offer protection to SARS-CoV-2 infection.

DISCUSSION

In this report, we present data on antibody modulation of Spike-monocyte interactions. A previously published report showed Spike-bead phagocytosis after opsonization with 50% heat-inactivated serum and a 16 hours incubation of beads with THP-1 cells (22). We believe that the data from our experiments are more representative of the first few events after

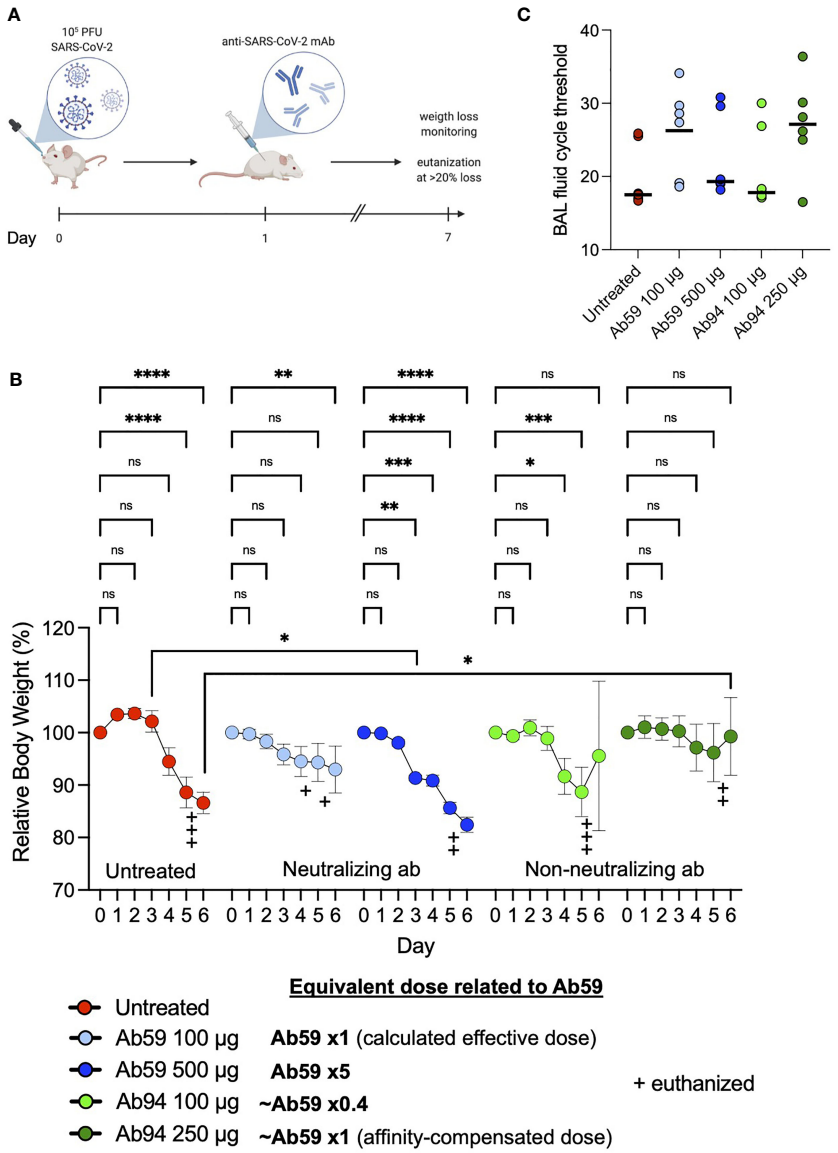

FIGURE 6 | Non-neutralizing antibodies can protect against SARS-CoV-2 infection. **(A)** Humanized ACE2 mice were infected intranasally with SARS-CoV-2 (Wuhan strain). One day after infection, the animals (N=7 per group) were treated intraperitoneally with antibodies. Relative body weights were recorded and tabulated. **(B)** Body weights relative to each individual mouse over the time course of viral infection and treatment. **(C)** Quantitative PCR analysis was performed on the BAL fluids obtained from the infected mice at the experiment termination. The cycle threshold (Ct) values were detected and graphed. Error bars represent the SD. Statistical significance was assessed using two-way ANOVA with Dunnett's multiple comparison correction both within each treatment group and across the groups for each day. * denotes $p \leq 0.05$, ** for $p \leq 0.01$, *** for $p \leq 0.001$ and **** for $p \leq 0.0001$. ns, not significant. Created with BioRender.com.

Spike-monocyte contact. Phagocytosis of small particles such as virions is a process that takes minutes, not hours (28). That is why we use shorter incubation times (30 min) and perform dose-response analysis across varying plasma concentrations. The dose-response analysis we performed exposed an antibody-mediated modulation of the Spike-monocyte interactions. It is important to elaborate on the concentrations we utilized, be it for plasma or monoclonal antibodies. For plasma, as tissues have a lower concentration of plasma proteins than whole blood, we used 1% as the highest concentration. As for the monoclonal antibody concentrations, we used 100 µg/ml as the highest concentration because it is roughly 1% of the antibody concentration present in plasma (10 mg/ml). Even though most of the experiments in this study are performed *in vitro*, we believe the effects we observe on phagocytosis efficiency could also be relevant *in vivo*, as the modulation effects occur already at relatively low antibody concentrations and would thus cover many physiological niches and scenarios.

The closest known phenomenon to the Spike-dependent phagocytosis modulation that we describe is the "Hook" or "prozone" effect. The prozone effect is a drop in antibody protection efficacy seen at very high concentrations. The prozone effect has been recognized in experiments with pneumococci, *Cryptococcus neoformans*, varicella and malaria (29–32). The mechanism is not known, but it has not been attributed to a reduction in phagocytosis per se (30) but rather to the creation of a proteinaceous coat on the organism surface, shielding them from immune recognition. Upon closer examination, we did notice a mild phagocytic differential when high antibody concentration was used in the published experiments (30). It is possible that other pathogens have evolved similar ability, and potentially through different mechanisms. That an increased binding of antibodies to a prey results in reduced or blocked phagocytosis is in contrast to the typically expected saturation at high opsonization levels, as what we and others have observed with the same type of experiment (same beads and cells) at even higher antibody concentrations (33). It cannot be explained by specific monoclonal interactions, as it is seen across diverse monoclonals as well as in convalescent polyclonal samples. It is important to note that we do not observe a Hook effect in any experiments (binding, neutralization etc.), except for phagocytosis. Also, in our experiments, the observed block in phagocytosis is only related to Spike protein and Spike-specific antibodies.

A combination of known mechanisms could potentially explain how SARS-CoV-2 could avoid phagocytosis using Spike protein. Bivalent trans-binding of antibodies is known to promote virion phagocytosis (34), where antigens are cross-linked depending on their density at the surface. Spike protein density on SARS-CoV-2 varies (35), and is increased with the D614G mutation (36). An increase in Spike antibody levels would lead to a competition of epitope binding, ultimately favoring the switch from bivalent trans-binding to monovalent binding, potentially leading to a reduction in phagocytosis. A synergistic mechanism could further aid SARS-CoV-2. Antigen height (especially below ~10 nm) is important for efficient phagocytosis (37), and most likely, a consistent antigen height is beneficial as well. Besides altering its density, SARS-CoV-2 also appears to be able to dramatically change the Spike protein conformation, where some proteins stand up vertically from the surface, and others are tilted down horizontally (35). At high anti-Spike levels, this would present an approaching phagocyte with a monovalently opsonized, irregular surface with variable antigen height (~15-25 nm), making the interaction difficult. In contrast, at low anti-Spike levels, the antibodies would be able to clasp Spike proteins in a bivalent, upright manner, presenting the phagocyte with a coherently opsonized surface at an effectively low antigen height. Careful mechanistic studies are needed to test this hypothesis.

How does the concentration-dependent phagocytosis modulation translate into an infection model? We utilized our anti-Spike antibodies as a therapeutic regimen in our animal infection. This creates a scenario where the mouse is already fighting the infection before therapy gets administered. The requirements, therefore, on therapeutic antibodies are higher than on prophylactic ones. When comparing the 100-μg dose of Ab59 and Ab94 (equivalent to 2.5 times lower binding affinity), we noticed that Ab59 showed better protection than the latter antibody. This could be attributed to either the neutralizing activity of Ab59, which Ab94 lacks, or the lower effective dose, given the lower Spike binding affinity of Ab94. Consistent with our data on phagocytosis (**Figure 5**), animals treated with the high dose of Ab59 (500 μg) fared worse than the animals that got the 100-μg dose. Interestingly, the animals that got the affinity-corrected dose for Ab94 (250 μg, equivalent to 100 μg of Ab59 in terms of binding affinity) fared the best in our cohort. The animal infection data on Ab94 protecting the mice is, most importantly, congruent with the phagocytosis data, indicating a role in infection management for non-neutralizing antibodies. In our double-blinded animal experiments, the weight loss kinetics seen is similar to other results (38), where they also analyzed viral load and lung pathology. We used the clinical standard assay for viral load assessment. Our cycle threshold values also showed that BAL viral load followed weight loss results in those animals which had better outcomes. This correlation shows that weight loss can be used to monitor the animal response to SARS-CoV-2 infection. In future studies, it remains to be established how infections would proceed in animals treated with an excessive dose of non-neutralizing antibodies. Our animal experiments show that monoclonal antibodies could be viable therapeutics even if they lack neutralizing potential.

It is widely accepted that a strong positive correlation exists between COVID19 disease severity and antibody titers (39–42). High antibody titers are generally associated with severe disease and hospitalization. The high titers are thought to be a consequence of the severe infection. Our results pose a new question: could the high anti-Spike titers seen in hospitalized patients instead (at least partially) contribute to the immune dysregulation and worsening patient outcomes? These questions are relevant in the light of the FDA's recommendation not to use monoclonal antibodies in hospitalized COVID19 patients (and who are seropositive) due to possible worsening of symptoms (3, 5). At the same time, it is important to note that convalescent plasma treatment for COVID19 was shown to be neither beneficial nor detrimental (43).

The dose variation data from Ab59-treated mice reflect the concentration-dependent modulation of Spike-bead phagocytosis. These results may explain the clinical findings seen in antibody therapy trials in the sense that having a low or excessive dosage of antibodies offers no clinical benefit (44). Recently, it has been alluded to that the differential effects seen across antibody treatment dosage in the Eli Lilly LY-CoV555 trial (44) were due to prozone-like effects (45). The authors of the clinical trial seem to disagree with the conclusions of the correspondence [please see the response from the authors in the same reference (45)]. Our results show a similar dose-dependent outcome differential as seen in the Ly-CoV555 clinical study, and suggest that a prozone-like effect could be relevant during monoclonal antibody treatment of SARS-CoV-2. Potentially, the mechanism could then be related to an antibody:

Spike-driven reduction in phagocytosis, but remains to be explained.

Coronaviruses are mutation prone (as has been the case with SARS-CoV-2), and our data indicate that non-neutralizing antibodies confer immune function *via* phagocytosis. This opsonic capability could potentially explain why anti-Spike antibodies generated even by older-generation vaccines or natural immunity can still offer protection against mutated variants (such as Beta and Delta) (46, 47). Phagocytosis, however, is not the only immune function mediated by antibodies in viral infections. Virion, as well as cellular phagocytosis and antibody-mediated killing, serve crucial roles in infection control. All those functions are independent of neutralization and can still be performed by antibodies against domains outside the RBD of Spike.

Overall, the results presented in this study highlight a concentration-dependent modulation of phagocytosis by anti-Spike antibodies. This modulation phenomenon might help explain the unclear clinical benefit seen with monoclonal antibody treatment for COVID19. This modulation is seen in patient material and translates well to animal infection experiments. The biophysical mechanism underlying the antibody-mediated phagocytic modulation is an exciting topic to pursue, as are the bridging immune steps between phagocytosis and animal protection.

MATERIALS AND METHODS

Cell Culture, Transfection, and Protein Production

THP-1 cells were maintained in RPMI medium supplemented with 10mM L-Glutamine and 10% fetal bovine serum (FBS). The cells were split kept at a density between $5x10^5$ and 10^6 cells/ml. The cells were split when they reached a density of 10^6 cells/ml, down to $5x10^5$ cells/ml. HEK293 cells (Sigma Aldrich 12022001-1VL) were maintained in DMEM supplemented with L-glutamine and 10% FBS. The cells were kept at 90% confluence and were not allowed to grow past passage 20. The plasmids for the 96 antibodies were aliquoted into 96 well plates. The cells to be transfected were grown in 24-well plates, with 500 µl of tissue culture medium. The plasmids were transfected into adherent HEK293 cells using the PEI method (48). The day after transfection the cell culture supernatant media was replaced with serum-free OptiMEM medium for 2 extra days. The supernatants containing the antibodies were distributed also in 96 well plates and stored for maximum one week for experimental use. HEK293 cells constitutively expressing the ACE2 receptor were acquired from BEI resources (NR-52511). They were maintained in DMEM supplemented with L- glutamine and 10% FBS for a maximum of 12 passages before being discarded. Expi293F suspension cells were purchased from Gibco (ThermoFisher) and routinely cultured in 125 ml Erlenmeyer flasks (Nalgene) in 30 ml Expi293 medium (Gibco) in an Eppendorf s41i shaker incubator at 37°C, 8% CO_2, 120 rpm. Cells were passaged and split to a density of 0.5 x 10^6 cells/ml every 3 to 4 days. The day before transfection, the cells were seeded at a density of 2 x 10^6 cells/ml. The next day, cells were seeded at 7.5 x 10^7 cells in 25.5 ml Expi293 medium. The transient transfection was carried out using 100 µl of Expifectamine (Gibco) according to the manufacturer's instructions. For Spike protein production, we used 40 µg of the Spike CS/PP plasmid (generously donated by Dr. Florian Krammer's lab). For antibody production, 20 µg of plasmids for the heavy and light chain was used, respectively. For all plasmids, 16 hours after transfection, 150 µl of enhancer 1 and 1.5 ml of enhancer 2 (Expifectamine transfection kit, Gibco) were added and cells cultured for an additional 3 days. The cells were then pelleted at 400 x g, 5 min, RT and the supernatant transferred to new tubes. Magne Protein G beads (Promega) were used to purify the antibodies according to the manufacturer's instructions.

Antibody Phage Selections

SARS-CoV-2 Spike RBD-specific scFv were selected by phage display technology from a human synthetic scFv library (49), similar in design and construction to previously reported (50). Briefly, selection of specific binders was performed through a process similar to the one described in the past (50) using biotinylated proteins SARS-CoV-2 S1 protein, His, Avitag™ (ACRO Biosystems, # S1N-C82E8) and SARS-CoV-2 Spike RBD, His, Avitag™ (ACRO Biosystems, # SPD-C82E9) immobilized on paramagnetic beads (Dynabeads M-280 streptavidin; Invitrogen Dynal AS, Oslo, Norway) as target antigen. Phagemid DNA from the third and fourth rounds of phage selection was isolated (Plasmid Miniprep kit, Qiagen) and the genes encoding scFv fragments were ligated into an in-house constructed screening vector providing the secreted scFv with a triple-FLAG tag and a hexahistidine (His_6) tag at the C-terminus. The constructs were subsequently transformed into TOP10 *E. coli* and individual, soluble scFv were produced as described elsewhere (50). Binding of individual selected scFv was initially assessed by ELISA against biotinylated antigen. Seven scFvs specific for RBD isolated this way were used to map relative epitope location of human IgG. The scFvs bind four epitopes on RBD, and two of them (A03-D03 and E01-C09) also interfere with the RBD-ACE2 interaction (data not shown).

COVID19 Patient Samples and B Cell Isolation

For the spike-THP-1 association experiments, 20 patients who had mild, moderate or severe COVID19 were asked to donate blood 6 weeks after infection diagnosis. Patients were classified into mild, moderate and severe COVID19 based on supportive respiratory treatment. Patients with mild COVID19 did not require oxygen treatment. Patients with moderate COVID-19 required supplementary oxygen support wheras patients with severe covid19 required non-invasive ventilation or high-flow nasal cannula oxygen therapy. All participants gave written informed consent to participate in the study which was approved by the Swedish ethical review authority (2020/01747). Blood was drawn in citrated tubes and plasma was

stored in the -80°C. For B cell isolation and antibody discovery, patients convalescing after severe COVID19 infection donated blood 6 weeks after discharge from the hospital. Thirtyml of blood were drawn into citrated tubes and the B cells were directly isolated using Rosettesep B (according to the manufacturer's instructions) and frozen at -150°C. B cells were harvested from 7 donors and were kept frozen until the sorting day when 10^7 cells were thawed, pooled and prepared for baiting which was performed in PBS +2% FBS. Spike protein (S1+S2 ECD-His Recombinant Protein) was purchased from SinoBiologicals (cat: 40589-V08B1) and was reconstituted to 1 mg/ml in PBS. Spike protein was conjugated to Alexafluor 647 microscale labeling kit (Invitrogen). The fluorescently labelled spike protein was incubated with the pooled B cells at a concentration of 0.5 µg/ml for 30 mins on ice. The cells were then washed with PBS, blocked in 2% BSA and stained with antibodies against CD19-PE (BD-555413), CD3-BV510 (BD-564713), IgG-BV421 (BD-562581) and a live/Dead Sytox stain. The cells were stained for 30 mins on ice and were later washed and prepared for sorting. Bulk cell sorting was performed using a FACSAriaFusion sorter, where the gates were set using unstained and FMO-1 controls. 7000 spike-reactive cells were sorted into RPMI + 10% FBS and were transported immediately to the RNA-sequencing facility while on ice.

10X Genomics Sequencing and Data Analysis

We performed 10X Genomics single-cell sequencing on the 7000 Spike-reactive cells (Center for Translational Genomics facility, Lund University). Cellranger suite cellranger mkfastq was used for demultiplexing and cellranger vdj for generating V(D)J sequences and annotation. Once received, we collated the V(D)J regions from our antibodies of interest using the V-Loupe software (10X Genomics software platform). 96 antibodies were chosen based on their phylogenetic distribution and the light and heavy chain variable regions were cloned into an IgG1 expression vector (Twist Biosciences). The 192 antibody plasmids (light and heavy chain constructs) were transformed into chemically competent Mix'n'go *E. coli* (Zymo research, T3002) and minipreps were prepared from the resultant colonies. Multiple sequence alignment using the ClustalW algorithm was performed on the light chain sequences and the heavy chain sequences. Single-linkage clustering was performed using the sum of the Hamming distances between the aligned light chain and the heavy chain as the similarity metric

Antibody Reactivity Screening

For ELISA, 10 µg/ml of Spike protein diluted in PBS was immobilized onto ELISA wells overnight at 4°C. The wells were washed with PBST and 100 µl of antibody supernatants were added to each well. A negative control (normal human pooled serum) and positive control (COVID patient serum) were used at 10% dilutions (in PBS). After one hour of incubation at 37°C, the wells were washed and HRP-conjugated protein G (Biorad 1706425) was added and kept for one hour at 37°C. The wells were finally washed and developed with 100 µl developing reagent (20 ml Substrate buffer NaCitrate pH 4.5 + 1 ml ABTS Peroxide substrate + 0.4 ml H2O2). OD_{450} was recorded and plotted.

For bead-based screening, fluorescent (APC) streptavidin microsphere beads (1 µm, Bangs Laboratories, Cat: CFR004) were used as Spike carriers. Spike protein was conjugated to biotin using the EZ-Link™ Micro Sulfo-NHS-LC-Biotinylation Kit (Thermofischer; Cat: 21935). The biotinylated Spike protein was attached to the streptavidin microbeads according to the bead manufacturer's instructions. For antibody reactivity testing, the Spike-beads were blocked with 5% BSA (in PBS) for 30 mins at 37°C. 150k beads were then centrifuged and incubated with 1 μ g/ml of antibody for one hour at 37°C in 96-well plates. The beads were washed with PBS and a secondary Alexa Fluor 488 conjugated Fab -Fab antibody (Jackson laboratories) was used to develop fluorescent signal. After a 30 min incubation with the secondary antibodies, the beads were further washed and fluorescence was detected using a Beckman Coulter Cytoflex flow cytometer.

Spike-THP-1 Association Assays

Spike-beads were opsonized with patient plasma or monoclonal antibodies at the specified concentrations for 30 minutes at 37°C in a 100 µl volume in 96 well plates. The beads were then centrifuged and reconstituted in 50 µl Sodium medium (5.6 mM glucose, 127 mM NaCl, 10.8 mM KCl, 2.4 mM KH_2PO_4, 1.6 mM $MgSO_4$, 10 mM HEPES, 1.8 mM $CaCl_2$; pH adjusted to 7.3 with NaOH). THP-1 cells were washed twice with PBS and reconstituted in Sodium medium. Spike beads and THP-1 cells were mixed at a ratio of 2 beads per THP-1 cell, in a final volume of 100 µl of Sodium medium. The suspension was mixed and cooled on ice for 5 minutes before incubating at 37°C in a shaking incubator for 30 minutes. The suspension was later cooled and analyzed *via* flow cytometry. Gating was first set on the cell population and the percentage of cells associated with beads (now fluorescent in the APC channel) was determined (**Figure 1A**). After cell-spike reactivity analysis was done, the cells were centrifuged and fixed with methanol (for 10 minutes at room temperature). The cells were then washed and resuspended in PBS, awaiting further flow cytometry analysis. Gates were then changed to include all the beads in the APC-fluorescent channel (**Figure 1B**, top right). For internalization analysis, Spike-beads were conjugated with pHrodo (FITC), an acid-sensitive dye that fluoresces in acidic environments. The beads were opsonized with different concentrations of antibodies and then interacted with THP-1 cells. Cells determined to be fluorescent in the APC and FITC channels by flow cytometry have had internalized as well as associated beads.

Pseudotyped Virus Neutralization Assays

Pseudotyped lentiviruses displaying the SARS-CoV-2 pandemic founder variant (Wu-Hu-1) packaging a firefly luciferase reporter gene were generated by the co-transfection of HEK293T cells using Lipofectamine 3000 (Invitrogen) per the manufacturer's protocols. Media was changed 12-16 hours after transfection, and pseudotyped viruses were harvested at 48- and 72-hours post-transfection, clarified by centrifugation, and

stored at -80°C until use. Pseudotyped viruses sufficient to generate ~50,000 relative light units (RLUs) were incubated with serial dilutions of antibodies for 60 min at 37°C in a 96-well plate, and then ~15,000 HEK293T-hACE2 cells were added to each well. For these experiments, the HEK293-ACE2 cell culture was supplemented with penicillin/streptomycin antibiotics to avoid contamination. Plates were incubated at 37°C for 48 hours, and luminescence was then measured using Bright-Glo (Promega) per the manufacturer's protocol, on a GM-2000 luminometer (Promega).

Bead-Based Neutralization Assay

HEK293-ACE2 cells were seeded at density of 35,000 cells per well in a Poly-D-Lysine coated flat bottom 96 well plate. The outer skirt wells were kept cell free and were filled with medium. The day of the experiment, Spike-beads were distributed to fresh 96 well plates, adding 700,000 beads/well. The beads were opsonized with 100 µl of antibody supernatants at 37°C for one hour. The beads were then resuspended by pipetting up and down and the bead/antibody mix was used to replace the medium on the HEK293-ACE2 cells. The cells were incubated with beads for one hour at 37°C. The cells then were washed three times with PBS and fixed with 4% paraformaldehyde at room temperature for 15 minutes. The cells were finally washed and prepared for imaging. Four images from the center of the field of each well in the 96-well plate were acquired using 10X magnification. The number of beads per field was automatically determined using the Nikon Jobs software. For each experiment, the average number of beads/quadrant per all 96 wells was calculated and used as a 100% reference. We chose to normalize our data internally this was because our hypothesis was that the majority of our antibodies would not be neutralizing. Data from four experiments were pooled and presented.

Animal Experiments

Forty-two nine-week old female K18 hACE2 (B6.Cg-Tg(K18-ACE2)2Prlmn/J) mice were inoculated intranasally with 10^5 PFU of SARS-CoV-2 (Wuhan strain, isolate SARS-CoV-2/01/human/2020/SWE, sourced from the Swedish Health Authorities). These mice are transgenic and carry the human ACE2 gene, making them permissive to SARS-CoV-2 infection (Jackson laboratories). One day after infection, the mice were split into 6 groups of 7 mice and antibodies were administered in one single dose intraperitoneally. We opted for a therapeutic model because we wanted to test the therapeutic potential of our antibodies under the most robust conditions. The body weights of the mice were recorded daily and the animals were euthanized if they lost more than 20% of their body weights or showed a severe deterioration in health status. The infection proceeded for 7 days before the animals were euthanized. Blood, tissue and bronchoalveolar lavage were harvested and stored accordingly. All the animal experiments were performed under the approval of the regional animal experimental ethics committee in Stockholm (16765–2020).

BAL Fluid qPCR Analysis

The bronchoalveolar lavage samples from mice were extracted using the MagNA pure 96 automated platform (Roche Life Science) followed by real-time RT-PCR-analysis of the SARS-CoV-2 envelope gene according to Corman et al, with some modifications (51). The thermal cycling was 48° for 10 min, then 95° for 10 min followed by 45 cycles of 95° for 15 s and 55° for 45 s. The PCR-analysis was performed using the Path-ID Multiplex one-step kit (Thermo-Fisher Scientific) and the 7500 Fast Real-time PCR system (Applied Biosystems).

Determination of IgG-Antigen Interaction Kinetics

Analysis of RBD-IgG reaction kinetics was performed on a MASS-16 biosensor instrument (Bruker, Hamburg, Germany). Anti-Human IgG (Fc) (Cytiva, Uppsala, Sweden) was diluted to 25 µg/ml in 10 mM sodium acetate buffer pH 5 and immobilized on a High Capacity Amine Sensor chip (Bruker) (time of interaction: 7 min; flow rate: 10 µl/min). S-protein-specific IgG was diluted in running buffer (Dulbecco's PBS (HyClone, South Logan, UT, USA) containing 0.01% Tween 20) and allowed to bind during a 90 s long injection (flow rate: 10 µl/min). Its capture level was set to be below 140 RU. The antigen (SARS-CoV-2 RBD (SinoBiological, Beijing, China; product number 40592-V08H) at 0.7-180 nM or Spike protein at 0.4-90 nM in running buffer) was subsequently injected (time of interaction: 2 min; flow rate: 30 µl/min). Dissociation was subsequently allowed to proceed for 5-15 min. The sensor chip was regenerated by treatment with 3 M magnesium chloride solution (Cytiva). All interactions were performed at 25°C. Apparent reaction rate kinetics was determined using a Langmuir 1:1 model using the Sierra Analyser software version 3.4.3 (Bruker).

Competition ELISA to Define Relative Epitope Location

High binding polystyrene 96-well plates (Corning Inc., Corning, NY, USA) were coated with 2 µg/ml streptavidin (Thermo Fisher Scientific, Waltham, MA, USA) diluted in Dulbecco's PBS (HyClone, South Logan, UT, USA) over night at +4°C. On the following day the plate was washed and subsequently incubated for 30 min with 30µl 30 nM biotinylated SARS-CoV-2 RBD (SinoBiological; product number:40592-V27H-B) diluted in Dulbecco's PBS containing 0.05% Tween 20 and 0.5% fish gelatine (Sigma Aldrich, St. Louis, MO, USA) (assay buffer). After washing the immobilized antigen was preincubated for 40 minutes at room temperature with 30 µl assay buffer or assay buffer containing 4.8 pmol IgG. Subsequently, 10 µl of assay buffer or assay buffer containing 4.8 pmol scFv was added to each well. After 1 hour incubation at room temperature the wells were washed and bound scFv was detected by incubation for 40 minutes at room temperature with peroxidase labelled monoclonal anti-FLAG® M2 antibody (Sigma Aldrich (30 µl diluted 1/4000 in assay buffer) and development using 1-Step™ Ultra TMB-ELISA Substrate Solution (Thermo Fisher Scientific).

Surface Plasmon Resonance Studies to Assess IgG-Specificity

The ability of IgG to interfere with the binding of SARS-CoV-2 RBD to its receptor, Angiotensin-Converting Enzyme 2 (ACE2) was examined by surface plasmon resonance-based detection in real time using a MASS-16 instrument (Bruker, Hamburg, Germany). The spots on a High Capacity Amine Sensor chip (Bruker) were immobilized with streptavidin (ThermoFisher Scientific, Waltham, MA, USA) (50 µg/ml diluted in 10 mM sodium acetate buffer pH 5.0; flow rate: 10 µl/min; time of immobilization: 6 min) to a level of approximately 1000 RU. Subsequently 50 nM biotinylated ACE2 (SinoBiological, Beijing, Shina; product number: 10108-H08H-B) was immobilized onto the chip's A spots (flow rate: 10 µl/s; time of binding: 2 min) while B spots were used as reference spots without ACE-2. 40 and 26 nM Receptor Binding Domain (RBD) was pre-incubated with 200 nM IgG diluted in Dulbecco's PBS (HyClone, South Logan, UT, USA) containing 0.01% Tween 20. The mixtures were injected over the sensor chip for 2 min, followed by a 6 min dissociation phase (flow rate: 30 µl/min). The sensor chip was regenerated by treatment with 1 M magnesium chloride solution (Sigma Aldrich, St Louis, MO, USA).

Binding of IgG to different mutated versions of SARS-CoV-2 was examined by a surface plasmon resonance assay. A High Capacity Amine Sensor chip (Bruker) was immobilized with F $(ab')_2$ Goat Anti-Human IgG, Fcγ fragment specific (Jackson, Ely, UK) at 50 µg/ml in 10 mM sodium acetate buffer pH 5 (time of interaction: 7 min; flow rate: 10 µl/min). Antibodies were diluted in Dulbecco's PBS (HyClone, South Logan, UT, USA) containing 0.01% Tween 20 and injected over the surface for 2 minutes at 10 µL/min. The antigens, produced in HEK293 cells, were obtained from SinoBiological (Beijing, China; product numbers: SARS-CoV-2 Spike RBD: 40592-V08H; SARS-CoV-2 Spike RBD-N501Y: 40592-V08H82; SARS-CoV-2 Spike RBD-E484K: 40592-V08H84; SARS-CoV-2 Spike RBD-K417N, E484K, N501Y: 40592-V08H85; SARS-CoV-2 Spike S1 HV69-70 deletion, Y144 deletion, N501Y, A570D, D614G, P681H: 40591-V08H12). All proteins were diluted to 50 nM in Dulbecco's PBS containing 0.01% Tween 20 and injected over the surface (time of interaction: 2 minutes; flow rate: 30 µl/min) followed by a dissociation phase of 6 minutes. After each cycle the surface was regenerated with 10 mM glycin pH 2.2 containing 30 mM HCl.

Crosslinking of Antibodies to Spike Protein

For the cross-linking of the antibodies to the Spike protein, 2 uG of each antibody was separately cross-linked to 2 uG of the Spike protein (Sino Biological Inc. 40589-V08H4 LC14SE2504, Recombinant SARS CoV-2 (1029-nCoV) Spike), as previously described (52). Briefly, the proteins were allowed to bind to each other in 50 uL of 1xPBS, pH 7.4 at 37°C, 500 rpm, 15 min. Heavy/light disuccinimidylsuberate (DSS; DSS-H12/D12, Creative Molecules Inc.) resuspended in dimethylformamide (DMF) was added to final concentrations 250 and 500 µM and incubated for a further of 60 min at 37°C, 800 rpm. The cross-linking reaction was quenched with a final concentration of 50 mM ammonium bicarbonate at 37°C, 800 rpm, 15 min.

Sample Preparation for MS

The cross-linked antibody-spike samples were denatured with 8 M urea - 100 mM ammonium bicarbonate, and the cysteine bonds reduced with a final concentration of 5 mM TCEP (37°C for 2h, 800 rpm) and subsequently alkylated with a final concentration of 10 mM iodoacetamide (22°C for 30 min, in the dark). The proteins were first digested with 1 µg of sequencing grade lysyl endopeptidase (Wako Chemicals) at 37°C, 800 rpm, 2h, diluted with 100 mM ammonium bicarbonate to a final urea concentration of 1.5 M, after which 1 µg sequencing grade trypsin (Promega) was added for further protein digestion (37°C, 800 rpm, 18 h). The samples were acidified to a final pH of 3.0 with 10% formic acid, and the peptides purified with C18 reverse phase spin columns according to the manufacturer's instructions (Macrospin columns, Harvard Apparatus). The peptides were dried in a speedvac and reconstituted in 2% acetonitrile, 0.2% formic acid prior to mass spectrometric analyses.

Liquid Chromatography Tandem Mass Spectrometry (LC-MS/MS)

All peptide analyses were performed on Q Exactive HF-X mass spectrometer (Thermo Scientific) connected to an EASY-nLC 1200 ultra-high-performance liquid chromatography system (Thermo Scientific), essentially as described with some minor modifications (PMID: 33411763). The peptides were loaded onto an Acclaim PepMap 100 (75µm x 2 cm) C18 (3 µm, 100 Å) pre-column and separated on an EASY-Spray column (Thermo Scientific; ID 75µm x 50 cm, column temperature 45°C) operated at a constant pressure of 800 bar. A linear gradient from 4 to 45% of 80% acetonitrile in aqueous 0.1% formic acid was run for 65 min at a flow rate of 350 nl min-1. One full MS scan (resolution 60000 @ 200 m/z; mass range 390–1 210m/z) was followed by MS/MS scans (resolution 15000 @ 200 m/z) of the 15 most abundant ion signals. The precursor ions were isolated with 2 m/z isolation width and fragmented using HCD at a normalized collision energy of 30. Charge state screening was enabled, and precursors with an unknown charge state and a charge state of 1 were rejected. The dynamic exclusion window was set to 10 s. The automatic gain control was set to 3e6 and 1e5 for MS and MS/MS with ion accumulation times of 110 ms and 60 ms, respectively. The intensity threshold for precursor ion selection was set to 1.7e4.

Computational Modeling

The variable domains (V_H-V_L) of antibodies were *de-novo* modeled and the sidechains were relaxed using Rosetta antibody (53) and relax protocols (54), respectively, from Rosetta software suite (26). For each epitope-paratope mapping, 2000 docking models were generated using Rosetta docking protocol (55) between the closed conformation of Spike protein (PDB id: 6VXX) and variable domain of target antibody. For ab66 specifically, the open conformation of Spike protein (PDB id: 7CAK) was also evaluated. The docking models for each pairwise conformation was filtered out through TX-MS protocol (25) using constraints derived from cross linking mass spectrometry experiments.

DATA AVAILABILITY STATEMENT

The raw data supporting the conclusions of this article will be made available by the authors, without undue reservation.

ETHICS STATEMENT

All participants gave written informed consent to participate in the study which was approved by the Swedish ethical review authority (2020/01747). The patients/participants provided their written informed consent to participate in this study. All the animal experiments were performed under the approval of the regional animal experimental ethics committee in Stockholm (16765–2020).

AUTHOR CONTRIBUTIONS

Conceptualization: WB, VW-H, RW, JM, LM, MO, MR, and PN. Experimentation and data analysis: WB, SW, MS, AB, UH, OL, HK, MG, MW, EE, ASS, LH, OA, JK, and TH. Writing original draft: WB and PN. All authors contributed to reading and editing the final manuscript.

FUNDING

WB, LM, JM, and PN are funded by the Knut and Alice Wallenberg Foundation. TH and equipment were funded by IngaBritt och Arne Lundbergs Forskningsstiftelse. WB, MO, JM, MR, and PN were funded by grants from the SciLifeLab National COVID-19 Research Program, financed by the Knut and Alice Wallenberg Foundation. WB was funded by the Royal Physiographic Society. HK was funded by Swiss National Science Foundation (grant no. P2ZHP3_191289).

ACKNOWLEDGMENTS

We thank Åsa Petersson for help with flow sorting and Berit Olofsson for technical assistance. We thank Benjamin Murrell and Daniel Sheward at the Karolinska Institutet for help with the pseudovirus neutralization assay. We thank Ali Mirazimi at the Public Health Agency of Sweden and Karolinska Institutet, for providing virus for the animal infection experiments performed. We thank the Department of Clinical Microbiology, Laboratory Medicine, Skåne University Hospital Lund for the qPCR analysis of BAL viral loads. We thank the Lund University Bioimaging Centre (LBIC) for use of fluorescence microscopes.

SUPPLEMENTARY MATERIAL

The Supplementary Material for this article can be found online at: https://www.frontiersin.org/articles/10.3389/fimmu.2021.808932/full#supplementary-material

REFERENCES

1. The IMpact-RSV SG. Palivizumab, a Humanized Respiratory Syncytial Virus Monoclonal Antibody, Reduces Hospitalization From Respiratory Syncytial Virus Infection in High-Risk Infants. *Pediatrics* (1998) 102:531–7. doi: 10.1542/peds.102.3.531
2. Mulangu S, Dodd LE, Davey RT, Tshiani Mbaya O, Proschan M, Mukadi D, et al. A Randomized, Controlled Trial of Ebola Virus Disease Therapeutics. *N Engl J Med* (2019) 381:2293–303. doi: 10.1056/NEJMoa1910993
3. FDA. *Fact Sheet For Health Care Providers Emergency Use Authorization (EUA) OF Regen-Covtm (Casirivimab With Imdevimab)* (2021). Available at: https://www.fda.gov/media/145611/download (Accessed May 25, 2021).
4. Gottlieb RL, Nirula A, Chen P, Boscia J, Heller B, Morris J, et al. Effect of Bamlanivimab as Monotherapy or in Combination With Etesevimab on Viral Load in Patients With Mild to Moderate COVID-19: A Randomized Clinical Trial. *JAMA* (2021) 325:632–44. doi: 10.1001/jama.2021.0202
5. FDA. *Emergency Use Authorization (EUA) OF Bamlanivimab And Etesevimab Authorized Use* (2021). Available at: https://www.fda.gov/media/145802/download#:~:text=The%20U.S.%20Food%20and%20Drug,patients%20(12%20years%20of%20age (Accessed May 25, 2021).
6. Taylor PC, Adams AC, Hufford MM, de la Torre I, Winthrop K, Gottlieb RL. Neutralizing Monoclonal Antibodies for Treatment of COVID-19. *Nat Rev Immunol* (2021) 21:382–93. doi: 10.1038/s41577-021-00542-x
7. Wu Y, Wang F, Shen C, Peng W, Li D, Zhao C, et al. A Noncompeting Pair of Human Neutralizing Antibodies Block COVID-19 Virus Binding to its Receptor ACE2. *Science* (2020) 368:1274–8. doi: 10.1126/science.abc2241
8. Cao Y, Su B, Guo X, Sun W, Deng Y, Bao L, et al. Potent Neutralizing Antibodies Against SARS-CoV-2 Identified by High-Throughput Single-Cell Sequencing of Convalescent Patients' B Cells. *Cell* (2020) 182:73–84.e16. doi: 10.1016/j.cell.2020.05.025
9. Ju B, Zhang Q, Ge J, Wang R, Sun J, Ge X, et al. Human Neutralizing Antibodies Elicited by SARS-CoV-2 Infection. *Nature* (2020) 584:115–9. doi: 10.1038/s41586-020-2380-z
10. Wang S, Peng Y, Wang R, Jiao S, Wang M, Huang W, et al. Characterization of Neutralizing Antibody With Prophylactic and Therapeutic Efficacy Against SARS-CoV-2 in Rhesus Monkeys. *Nat Commun* (2020) 11:5752. doi: 10.1038/s41467-020-19568-1
11. Yamayoshi S, Yasuhara A, Ito M, Akasaka O, Nakamura M, Nakachi I, et al. Antibody Titers Against SARS-CoV-2 Decline, But do Not Disappear for Several Months. *EClinicalMedicine* (2021) 32:100734. doi: 10.1016/j.eclinm.2021.100734
12. Forthal DN. Functions of Antibodies. *Microbiol Spectr* (2014) 2:1–17. doi: 10.1128/microbiolspec.AID-0019-2014
13. Huber VC, Lynch JM, Bucher DJ, Le J, Metzger DW. Fc Receptor-Mediated Phagocytosis Makes a Significant Contribution to Clearance of Influenza Virus Infections. *J Immunol* (2001) 166:7381–8. doi: 10.4049/jimmunol.166.12.7381
14. Fujisawa H. Neutrophils Play an Essential Role in Cooperation With Antibody in Both Protection Against and Recovery From Pulmonary Infection With Influenza Virus in Mice. *J Virol* (2008) 82:2772–83. doi: 10.1128/JVI.01210-07
15. Keeler SP, Fox JM. Requirement of Fc-Fc Gamma Receptor Interaction for Antibody-Based Protection Against Emerging Virus Infections. *Viruses* (2021) 13(6). doi: 10.3390/v13061037
16. Khandia R, Munjal A, Dhama K, Karthik K, Tiwari R, Malik YS, et al. Modulation of Dengue/Zika Virus Pathogenicity by Antibody-Dependent Enhancement and Strategies to Protect Against Enhancement in Zika Virus Infection. *Front Immunol* (2018) 9:597. doi: 10.3389/fimmu.2018.00597
17. Karthik K, Senthilkumar TMA, Udhayavel S, Raj GD. Role of Antibody-Dependent Enhancement (ADE) in the Virulence of SARS-CoV-2 and its Mitigation Strategies for the Development of Vaccines and Immunotherapies

to Counter COVID-19. *Hum Vaccin Immunother* (2020) 16:3055–60. doi: 10.1080/21645515.2020.1796425
18. Logunov DY, Dolzhikova IV, Shcheblyakov DV, Tukhvatulin AI, Zubkova OV, Dzharullaeva AS, et al. Safety and Efficacy of an Rad26 and Rad5 Vector-Based Heterologous Prime-Boost COVID-19 Vaccine: An Interim Analysis of a Randomised Controlled Phase 3 Trial in Russia. *Lancet* (2021) 397:671–81. doi: 10.1016/S0140-6736(21)00234-8
19. Baden LR, El Sahly HM, Essink B, Kotloff K, Frey S, Novak R, et al. Efficacy and Safety of the mRNA-1273 SARS-CoV-2 Vaccine. *N Engl J Med* (2021) 384:403–16. doi: 10.1056/NEJMoa2035389
20. Voysey M, Clemens SAC, Madhi SA, Weckx LY, Folegatti PM, Aley PK, et al. Safety and Efficacy of the ChAdOx1 Ncov-19 Vaccine (AZD1222) Against SARS-CoV-2: An Interim Analysis of Four Randomised Controlled Trials in Brazil, South Africa, and the UK. *Lancet* (2021) 397:99–111. doi: 10.1016/S0140-6736(20)32661-1
21. Polack FP, Thomas SJ, Kitchin N, Absalon J, Gurtman A, Lockhart S, et al. Safety and Efficacy of the BNT162b2 mRNA Covid-19 Vaccine. *N Engl J Med* (2020) 383:2603–15. doi: 10.1056/NEJMoa2034577
22. Pierce CA, Preston-Hurlburt P, Dai Y, Aschner CB, Cheshenko N, Galen B, et al. Immune Responses to SARS-CoV-2 Infection in Hospitalized Pediatric and Adult Patients. *Sci Transl Med* (2020) 12(564). doi: 10.1126/scitranslmed.abd5487
23. Alter G, Yu J, Liu J, Chandrashekar A, Borducchi EN, Tostanoski LH, et al. Immunogenicity of Ad26.COV2.S Vaccine Against SARS-CoV-2 Variants in Humans. *Nature* (2021) 596:268–72. doi: 10.1038/s41586-021-03681-2
24. Díez JM, Romero C, Cruz M, Vandeberg P, Merritt WK, Pradenas E, et al. Anti-SARS-CoV-2 Hyperimmune Immunoglobulin Provides Potent and Robust Neutralization Capacity and Antibody-Dependent Cellular Cytotoxicity and Phagocytosis Induction Through N and S Proteins. *BioRxiv* (2021). doi: 10.1101/2021.06.11.447942
25. Hauri S, Khakzad H, Happonen L, Teleman J, Malmström J, Malmström L. Rapid Determination of Quaternary Protein Structures in Complex Biological Samples. *Nat Commun* (2019) 10:192. doi: 10.1038/s41467-018-07986-1
26. Leman JK, Weitzner BD, Lewis SM, Adolf-Bryfogle J, Alam N, Alford RF, et al. Macromolecular Modeling and Design in Rosetta: Recent Methods and Frameworks. *Nat Methods* (2020) 17:665–80. doi: 10.1038/s41592-020-0848-2
27. Benton DJ, Wrobel AG, Xu P, Roustan C, Martin SR, Rosenthal PB, et al. Receptor Binding and Priming of the Spike Protein of SARS-CoV-2 for Membrane Fusion. *Nature* (2020) 588:327–30. doi: 10.1038/s41586-020-2772-0
28. Nordenfelt P, Tapper H. Phagosome Dynamics During Phagocytosis by Neutrophils. *J Leukoc Biol* (2011) 90:271–84. doi: 10.1189/jlb.0810457
29. Felton L. The Units of Protective Antibody in Antipneumococcus Serum and Antibody Solution. *J Infect Dis* (1928) 43.
30. Taborda CP, Casadevall A. Immunoglobulin M Efficacy Against Cryptococcus Neoformans: Mechanism, Dose Dependence, and Prozone-Like Effects in Passive Protection Experiments. *J Immunol* (2001) 166:2100–7. doi: 10.4049/jimmunol.166.3.2100
31. Taborda CP, Rivera J, Zaragoza O, Casadevall A. More is Not Necessarily Better: Prozone-Like Effects in Passive Immunization With IgG. *J Immunol* (2003) 170:3621–30. doi: 10.4049/jimmunol.170.7.3621
32. Asano Y, Albrecht P, Stagno S, Takahashi M. Potentiation of Neutralization of Varicella-Zoster Virus to Antibody to Immunoglobulin. *J Infect Dis* (1982) 146:524–9. doi: 10.1093/infdis/146.4.524
33. de Neergaard T, Sundwall M, Wrighton S, Nordenfelt P. High-Sensitivity Assessment of Phagocytosis by Persistent Association-Based Normalization. *J Immunol* (2021) 206:214–24. doi: 10.4049/jimmunol.2000032
34. Klein JS, Bjorkman PJ. Few and Far Between: How HIV may be Evading Antibody Avidity. *PloS Pathog* (2010) 6:e1000908. doi: 10.1371/journal.ppat.1000908
35. Ke Z, Oton J, Qu K, Cortese M, Zila V, McKeane L, et al. Structures and Distributions of SARS-CoV-2 Spike Proteins on Intact Virions. *Nature* (2020) 588:498–502. doi: 10.1038/s41586-020-2665-2
36. Zhang L, Jackson CB, Mou H, Ojha A, Peng H, Quinlan BD, et al. SARS-CoV-2 Spike-Protein D614G Mutation Increases Virion Spike Density and Infectivity. *Nat Commun* (2020) 11:6013. doi: 10.1038/s41467-020-19808-4
37. Bakalar MH, Joffe AM, Schmid EM, Son S, Podolski M, Fletcher DA. Size-Dependent Segregation Controls Macrophage Phagocytosis of Antibody-Opsonized Targets. *Cell* (2018) 174:131–42.e13. doi: 10.1016/j.cell.2018.05.059
38. Winkler ES, Bailey AL, Kafai NM, Nair S, McCune BT, Yu J, et al. SARS-CoV-2 Infection of Human ACE2-Transgenic Mice Causes Severe Lung Inflammation and Impaired Function. *Nat Immunol* (2020) 21:1327–35. doi: 10.1038/s41590-020-0778-2
39. Klein SL, Pekosz A, Park H-S, Ursin RL, Shapiro JR, Benner SE, et al. Sex, Age, and Hospitalization Drive Antibody Responses in a COVID-19 Convalescent Plasma Donor Population. *J Clin Invest* (2020) 130:6141–50. doi: 10.1172/JCI142004
40. Garcia-Beltran WF, Lam EC, Astudillo MG, Yang D, Miller TE, Feldman J, et al. COVID-19-Neutralizing Antibodies Predict Disease Severity and Survival. *Cell* (2021) 184:476–488.e11. doi: 10.1016/j.cell.2020.12.015
41. Long Q-X, Liu B-Z, Deng H-J, Wu G-C, Deng K, Chen Y-K, et al. Antibody Responses to SARS-CoV-2 in Patients With COVID-19. *Nat Med* (2020) 26:845–8. doi: 10.1038/s41591-020-0897-1
42. Bläckberg A, Fernström N, Sarbrant E, Rasmussen M, Sunnerhagen T. Antibody Kinetics and Clinical Course of COVID-19 a Prospective Observational Study. *PloS One* (2021) 16:e0248918. doi: 10.1371/journal.pone.0248918
43. RECOVERY Collaborative Group. Convalescent Plasma in Patients Admitted to Hospital With COVID-19 (RECOVERY): A Randomised Controlled, Open-Label, Platform Trial. *Lancet* (2021) 397:2049–59. doi: 10.1016/S0140-6736(21)00897-7
44. Chen P, Nirula A, Heller B, Gottlieb RL, Boscia J, Morris J, et al. SARS-CoV-2 Neutralizing Antibody LY-CoV555 in Outpatients With Covid-19. *N Engl J Med* (2021) 384:229–37. doi: 10.1056/NEJMoa2029849
45. Casadevall A, Joyner MJ, Pirofski L-A. Neutralizing Antibody LY-CoV555 for Outpatient Covid-19. *N Engl J Med* (2021) 384:189. doi: 10.1056/NEJMc2033787
46. Lopez Bernal J, Andrews N, Gower C, Gallagher E, Simmons R, Thelwall S, et al. Effectiveness of Covid-19 Vaccines Against the B.1.617.2 (Delta) Variant. *N Engl J Med* (2021) 385:585–94. doi: 10.1056/NEJMoa2108891
47. Charmet T, Schaeffer L, Grant R, Galmiche S, Chény O, Von Platen C, et al. Impact of Original, B.1.1.7 and B.1.351/P.1 SARS-CoV-2 Lineages on Vaccine Effectiveness of Two Doses of COVID-19 mRNA Vaccines: Results From a Nationwide Case-Control Study in France. *Lancet Reg Health Eur* (2021) 8:100171. doi: 10.1016/j.lanepe.2021.100171
48. Longo PA, Kavran JM, Kim M-S, Leahy DJ. Transient Mammalian Cell Transfection With Polyethylenimine (PEI). *Meth Enzymol* (2013) 529:227–40. doi: 10.1016/B978-0-12-418687-3.00018-5
49. Preger C, Wigren E, Ossipova E, Marks C, Lengqvist J, Hofström C, et al. Generation and Validation of Recombinant Antibodies to Study Human aminoacyl-tRNA Synthetases. *J Biol Chem* (2020) 295:13981–93. doi: 10.1074/jbc.RA120.012893
50. Säll A, Walle M, Wingren C, Müller S, Nyman T, Vala A, et al. Generation and Analyses of Human Synthetic Antibody Libraries and Their Application for Protein Microarrays. *Protein Eng Des Sel* (2016) 29:427–37. doi: 10.1093/protein/gzw042
51. Corman VM, Landt O, Kaiser M, Molenkamp R, Meijer A, Chu DK, et al. Detection of 2019 Novel Coronavirus (2019-Ncov) by Real-Time RT-PCR. *Euro Surveill* (2020) 25(3). doi: 10.2807/1560-7917.ES.2020.25.3.2000045
52. Bahnan W, Happonen L, Khakzad H, Kumra Ahnlide V, de Neergaard T, Wrighton S, et al. Protection Induced by a Human Monoclonal Antibody Recognizing Two Different Epitopes in a Conserved Region of Streptococcal M Proteins. *BioRxiv* (2021). doi: 10.1101/2021.03.01.433494
53. Marze NA, Lyskov S, Gray JJ. Improved Prediction of Antibody VL-VH Orientation. *Protein Eng Des Sel* (2016) 29:409–18. doi: 10.1093/protein/gzw013
54. Conway P, Tyka MD, DiMaio F, Konerding DE, Baker D. Relaxation of Backbone Bond Geometry Improves Protein Energy Landscape Modeling. *Protein Sci* (2014) 23:47–55. doi: 10.1002/pro.2389
55. Marze NA, Roy Burman SS, Sheffler W, Gray JJ. Efficient Flexible Backbone Protein-Protein Docking for Challenging Targets. *Bioinformatics* (2018) 34:3461–9. doi: 10.1093/bioinformatics/bty355

Conflict of Interest: Authors UH and OL were employed by company Adlego Biomedical AB. Author VW-H was employed by company Tanea Medical AB. Author RW was employed by company SciEd Solutions.

The remaining authors declare that the research was conducted in the absence of any commercial or financial relationships that could be construed as a potential conflict of interest.

Publisher's Note: All claims expressed in this article are solely those of the authors and do not necessarily represent those of their affiliated organizations, or those of the publisher, the editors and the reviewers. Any product that may be evaluated in

this article, or claim that may be made by its manufacturer, is not guaranteed or endorsed by the publisher.

Copyright © 2022 Bahnan, Wrighton, Sundwall, Bläckberg, Larsson, Höglund, Khakzad, Godzwon, Walle, Elder, Strand, Happonen, André, Ahnlide, Hellmark, Wendel-Hansen, Wallin, Malmstöm, Malmström, Ohlin, Rasmussen and Nordenfelt.

This is an open-access article distributed under the terms of the Creative Commons Attribution License (CC BY). The use, distribution or reproduction in other forums is permitted, provided the original author(s) and the copyright owner(s) are credited and that the original publication in this journal is cited, in accordance with accepted academic practice. No use, distribution or reproduction is permitted which does not comply with these terms.